coatings

Article

Effect of WC on Microstructure and Wear Resistance of Fe-Based Coating Fabricated by Laser Cladding

Angang Wei [1], Yun Tang [2], Tong Tong [1,*], Fang Wan [2], Shaoshuai Yang [2] and Kaiming Wang [3,4,*]

1 China Huaneng Group Clean Energy Technology Research Institute Co., Ltd., Beijing 102209, China
2 Huaneng Huajialing Wind Power Co., Ltd., Lanzhou 730070, China
3 College of Automotive and Mechanical Engineering, Changsha University of Science and Technology, Changsha 410114, China
4 State Key Laboratory of Tribology in Advanced Equipment, Department of Mechanical Engineering, Tsinghua University, Beijing 100084, China
* Correspondence: t_tong@qny.chng.com.cn (T.T.); kmwang@csust.edu.cn (K.W.)

Abstract: As the core component of the wind turbine transmission chain, the wind power gear plays a vital role in the safe and efficient operation of the whole machine. Wind power gears are subjected to varying degrees of wear on their contact surfaces due to alternating load impacts. For wind power gear repair and remanufacturing, laser cladding technology is proposed on the wind power gearbospline shaft. The effect of tungsten carbide (WC) addition on the laser-clad Fe-based coatings was investigated in this study. The morphology and composition of the composite coatings formed with different proportions of WC were studied using scanning electron microscopy (SEM) and energy-dispersive spectroscopy (EDS). The microhardness and wear resistance were measured with a digital microhardness tester and a wear testing machine, respectively. The coatings were compact with no apparent cracks or pores and the microstructures of the regions above the fusion zone gradually changed from planar crystal to columnar crystal and cellular crystal, while the middle and upper parts of the coating mainly consisted of equiaxed crystals. The microhardness of the coatings gradually increased with the increase of WC content. The coating with 16% WC addition reached a maximum microhardness of 826.2 HV. The increase of WC content improved the wear resistance of the laser-clad Fe-based composite coatings. The wear mechanism of the coatings was mainly abrasive wear, along with slight adhesion wear and oxidative wear.

Keywords: wind power gears; laser cladding; Fe-based coating; microstructure; wear-resistance

check for updates

Citation: Wei, A.; Tang, Y.; Tong, T.; Wan, F.; Yang, S.; Wang, K. Effect of WC on Microstructure and Wear Resistance of Fe-Based Coating Fabricated by Laser Cladding. *Coatings* **2022**, *12*, 1209. https://doi.org/10.3390/coatings12081209

Academic Editor: Rafael Comesaña

Received: 10 July 2022
Accepted: 16 August 2022
Published: 18 August 2022

1. Introduction

The failure of wind turbine gearboxes accounts for 40% of the total failure of wind turbines, and is the primary cause of shutdown of wind turbines [1]. Due to the complex working conditions of gears and the huge load they are subjected to, gear wear is the leading cause of gearbox failure. The improvement of the wear resistance of gears is urgent to extend the lifespan of gearboxes and improve the overall power generation efficiency of wind turbines [2]. The methods commonly used at home and abroad to improve the wear resistance of components include laser cladding [3], shot peening [4], overlay welding [5] and thermal spraying [6]. All these technologies have a certain effect on the improvement of the wear resistance of wind power gears.

Laser cladding (LC) is an advanced surface modification technology which uses a laser as a heat source to melt the filler material (powder or wire) and the substrate together [7–11]. After solidification, an LC coating is formed on the substrate's surface, thus enhancing wear and/or corrosion resistance of the substrate [12–14]. LC has a high work efficiency, emits less pollution and can be used to fabricate thick coatings, all of which are advantages over other surface treatment techniques [15]. Moreover, LC can refine the grains and stabilize the phase owing to its rapid cooling rate [16]. In addition, laser-clad coatings generally display a low dilution rate and strong metallurgical bonding with the substrate [17]. Therefore, LC received much attention and became one of the hotspots in current research. LC is now widely studied and used in important fields such as aerospace, metallurgy and engineering machinery [18–20]. For example, Huebner et al. [21] fabricated the Inconel 625-WC composite coatings on Inconel 625 substrate via LC for turbine blade application. Tungsten carbide (WC) addition facilitated the formation of topologically close-packed phases and carbides, which improve the mechanical properties of the composite coatings and improve the performance of the die steel at high temperature. Cui et al. [16] fabricated $FeCoCrNiMnAl_x$ high-entropy alloy coatings on H13 steel via LC. The combined effects of improved microhardness and oxidation resistance enhanced the wear resistance of the $FeMnCrNiCoAl_x$ coatings at high temperature, which effectively protected the H13 substrate from wear. Zhu et al. [22] cladded 316L, 410 and 420 stainless steel coatings on rail wheel discs via LC to analyze their wear characteristics. Results revealed that all three clad wheel discs displayed lower wear rates compared to the unclad wheel discs.

At present, there are self-fusing alloy powders, ceramic powders, composite powders, etc. The self-fusing alloy powders, including Fe-based [23,24], Ni-based [25,26], Co-based [27,28], etc., refer to the powders with specific elements. Among them, the composition of Fe-based alloy powder is very similar to steel. When the substrate is steel, the two can be more compatible, forming a metallurgical bond with firm interfacial bonding. In addition, the cost of Fe-based alloy powder is very low, so it is widely used in LC. However, compared with Ni-based and Co-based alloy powders, Fe-based alloy powder displays poorer self-melting properties and relatively weaker corrosion resistance. The WC ceramic powder with high hardness exhibits excellent wear resistance properties, which can further improve the wear resistance of the LC coatings. Composite powder mainly refers to a composite or mixed powder system with ceramic and metal powders, and is currently a hot topic in the field of LC technology. Chen et al. [29] fabricated H13 steel matrix composites with TiC reinforced particles via LC. The effects of the TiC volume fraction on microstructure and hardness of the TiC/H13 composites were studied. Results showed that the hardness of TiC/H13 composites with 80% TiC (volume fraction) was two times higher than that of the H13 substrate. Ding et al. [30] conducted LC experiments on railway CL60 wheel steel using Fe-based powders with different WS_2 contents. The authors reported the smallest wear rate (2.7 μg/m) and the shortest rolling contact fatigue cracks that occurred on the coatings with 6 wt.% WS_2. Chen et al. [31] synthesized in-situ TiC and TiB_2 reinforced composite coatings on carbon steel to enhance the hardness as well as wear resistance of remanufactured components. Results revealed that the microhardness of composite coating with 961.49 HV is 5.04 times more, and the corresponding wear loss is 2.8 times less, than those of 45 steel.

In this study, the aims are to investigate the effect of tungsten carbide (WC) content on the morphology, microstructure and properties of Fe-based LC coatings. Therefore, the Fe-based LC coatings with WC addition on Q550 structural steel were prepared to improve the wear resistance and service life of wind turbine gears. The research results are expected to provide technical support for the repair and manufacture of wind turbine gears.

2. Materials and Methods

2.1. Materials

Q550 structural steel (Wuyang Iron and Steel Co., Ltd., Wugang, China) was selected as the LC substrate and its chemical composition is given in Table 1. The Fe-based alloy powder (BGRIMM Advanced Materials Science & Technology Co., Ltd., Beijing, China) with a particle size of 50~105 μm was utilized to prepare the LC coatings and its chemical composition is given in Table 2. The WC powder is a nickel-coated WC powder with 15.2 wt.% Ni content. The nickel-coated WC powder could improve the wettability and bonding strength between WC and the Q550 substrate. The Fe-based alloy powders with different WC contents (0%, 4%, 8%, 12% and 16% in mass ratio) were put into a ball mill

(QXQM-4) with a ball-to-powder ratio of 2:1. The speed of ball milling was set as 100 r/min for 2 h for evenly mixed Fe /WC composite powders.

Table 1. Chemical composition of Q550 structural steel.

Element	C	Si	Mn	P	S	Fe
wt.%	0.13–0.18	0.20–0.50	0.90–1.30	0.90–1.30	0.90–1.30	Bal.

Table 2. Chemical composition of Fe-based alloy powders.

Element	Cr	B	Si	C	Fe
wt.%	13.0	1.6	1.2	0.15	Bal.

2.2. Methods

The LC experiment was performed using a fiber laser (YLS-3000, IPG Photonics Corporation, Oxford, MA, USA) with a spot diameter of 1.8 mm with a coaxial powder feeder. Before the experiment, the surface of the substrate was ground with sandpaper to remove the surface oxides and enhance the bonding strength between the coating and substrate. The surfaces were then cleaned with ethanol to remove impurities and oil. The following optimized LC process parameters were used: laser power of 900 W, a scanning speed of 4 mm/s, a powder feeding rate of 8.5 g/min, a defocus amount of 20 mm and an overlap rate of 40%. 99.99% argon was used and the shielding gas flow was 15 L/min.

After LC, the oxide layers and slag on the coatings' surfaces were removed by sandpaper and the macroscopic morphologies of the coatings were then observed using a stereomicroscope (Leica S9i, Leica, Weztlar, Germany). The LC samples were cut from the middle using the electrical discharge machine. The surfaces perpendicular to the scanning direction were ground with 280#, 400#, 600#, 800#, 1000# and 1400# grit sandpapers in turn, and then polished.

The sample was etched for about 30 s using nitrate alcohol etching solution (HNO_3:HCL = 1:3). The microstructures of the coatings were observed via a scanning electron microscope (SEM, JSM-IT200, JEOL Ltd., Tokyo, Japan), which is equipped with energy dispersive spectroscopy (EDS, JEOL Ltd., Tokyo, Japan).

One piece of sample was used for hardness measurement and microstructural observation. The other was ground using a grinding machine before the wear tests. The semi-automatic Vickers hardness tester (HVST-1000Z, SHSIWEI, Shanghai, China) was utilized for hardness measurement. The load using for the hardness measurement is 15N. The average value of five random regions was defined as the hardness value of the coating.

A high-frequency reciprocating wear tester (MDW-05, Jinan Yihua Tribology Testing Technology Co., Ltd, Jinan, China) was used to test the wear properties of the coatings. The GCr15 balls, with a diameter of 6 mm, were selected as the grinding balls. The corresponding parameters were: a reciprocating distance of 5 mm, a frequency of 2 Hz, a normal load of 50 N and a testing time of 30 min. The wear loss was measured using an electronic balance with 0.1 mg precision. The worn surfaces were observed by SEM to analyze the wear mechanism.

3. Results and Discussion

3.1. Macroscopic Morphology

The macroscopic morphologies of the coatings with different WC contents are shown in Figure 1. It can be seen that the surface morphologies of the coatings were compact with no apparent cracks or pores, and there were no obvious powders sticking to the coating surface, which benefited from the previously optimized LC process parameters.

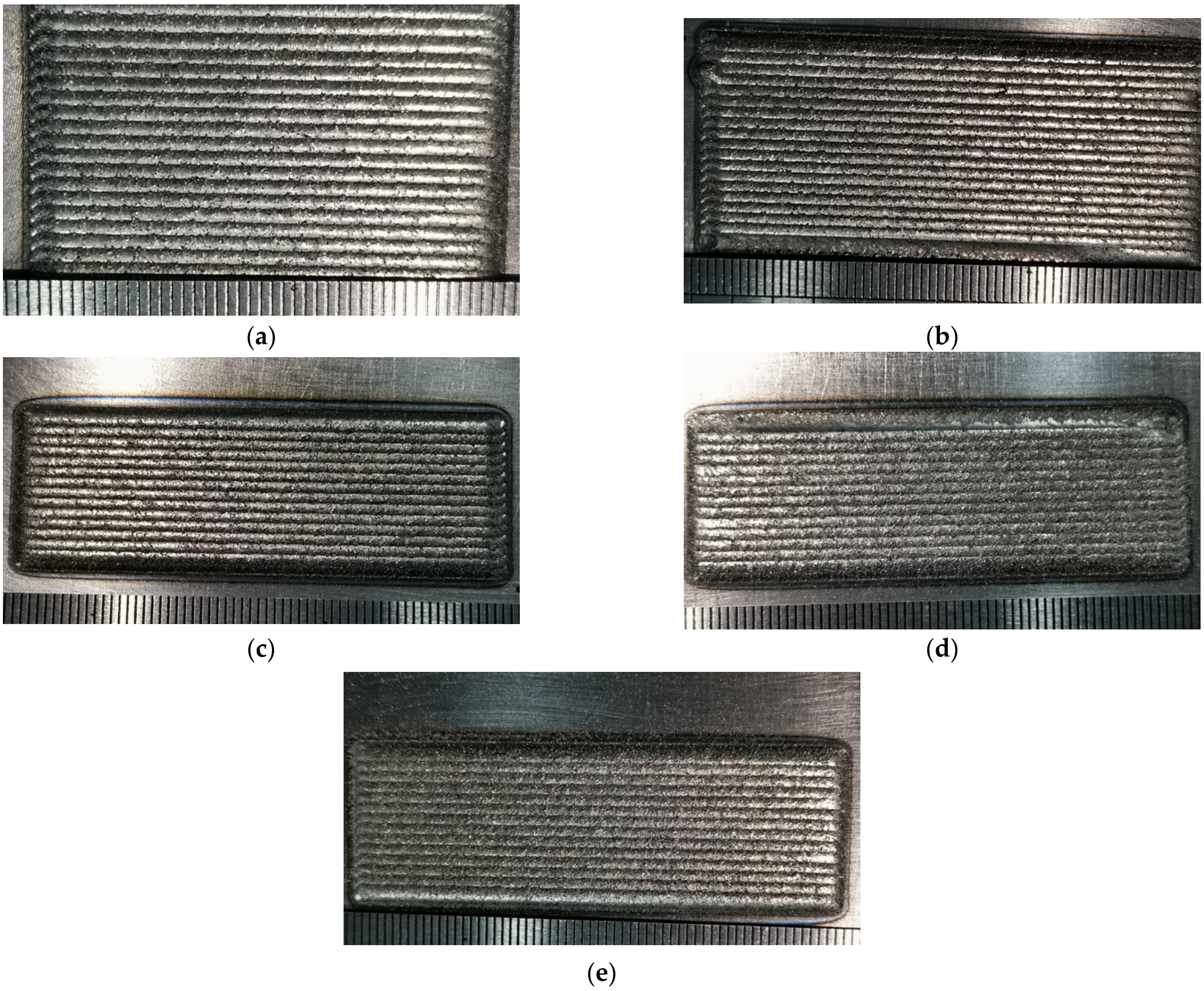

Figure 1. Macroscopic morphologies of the composite coatings with different WC contents: (**a**) 0 wt.% WC; (**b**) 4 wt.% WC; (**c**) 8 wt.% WC; (**d**) 12 wt.% WC and (**e**) 16 wt.% WC.

3.2. Microstructure

Figure 2 shows the microstructure of the LC Fe-based coatings with different WC contents. It can be seen that the microstructure of each coating exhibits a distinct difference as WC content changes. A white fusion zone appeared at the bottom of the coating, which indicates that the coating and the substrate have good metallurgical bonding. From the figure, it can be seen that the microstructures in the fusion zone were mainly planar crystals. The microstructures of the regions above the fusion zone gradually changed from planar crystal to columnar crystal and cellular crystal, while the middle and upper parts of the coating mainly consisted of equiaxed crystals. The microstructures inside the coating are mainly associated with temperature gradient (G) and solidification rate (R), analyzed in G/R [32]. At the initial stage of solidification, the temperature gradient of the fusion zone was relatively large, but the solidification rate was relatively low [33]. The G/R value of the fusion zone was large, so the microstructure was mainly planar crystal structure. As the solidification moved upward, the temperature gradient decreased, while the solidification rate increased, the G/R value decreased gradually, and the microstructure above the fusion zone gradually transformed into columnar and cellular crystals. The temperature gradient in the middle and upper parts of the coating further decreased, while the solidification rate continued to increase, leading to a decreased G/R value. Therefore, the microstructure in the middle and upper parts of the coating transformed into equiaxed grains. In addition, the grain size of the coating was gradually refined with increasing WC content. It is evident that the microstructures inside the heat-affected zone (HAZ) were mainly martensite. The

Q550 steel initially consisted of ferrite and pearlite. However, during LC, the temperature in HAZ exceeded the austenitizing temperature but did not reach the melting point of the Q550 steel. In the rapid cooling process, ferrite and pearlite in HAZ transformed into martensite [34].

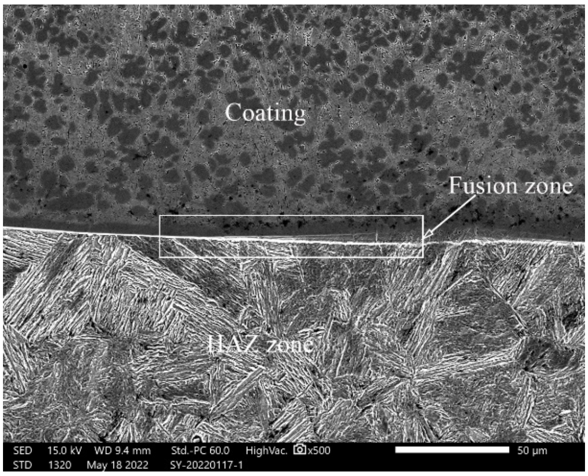

(**a**)

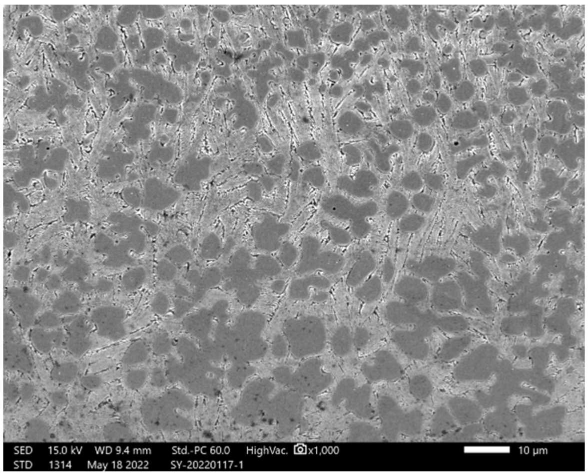

(**b**)

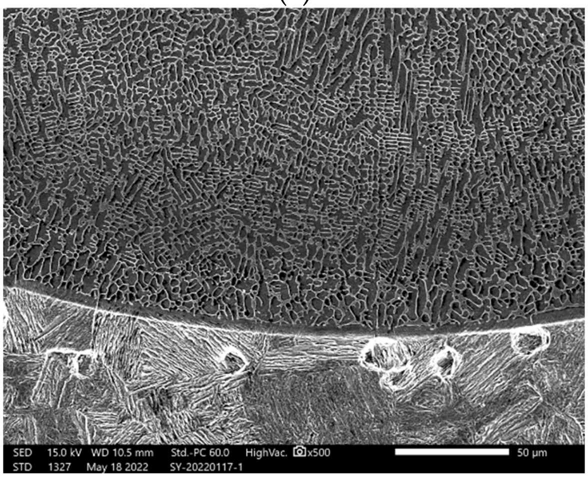

(**c**)

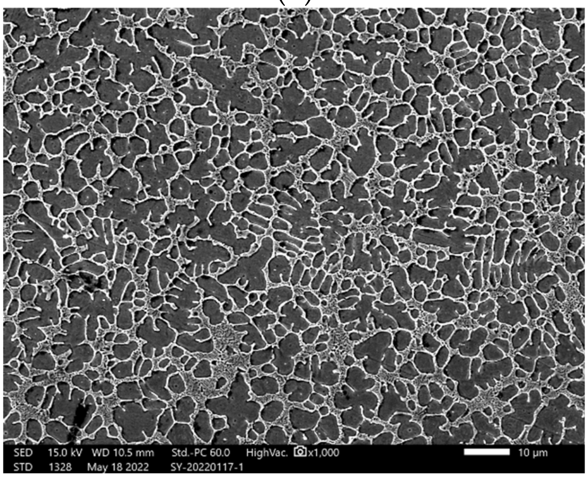

(**d**)

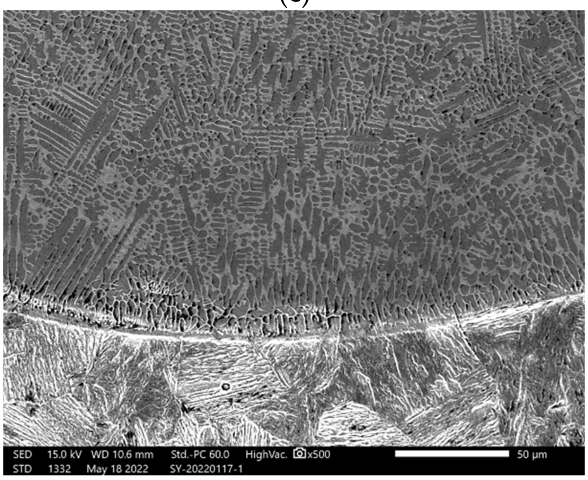

(**e**)

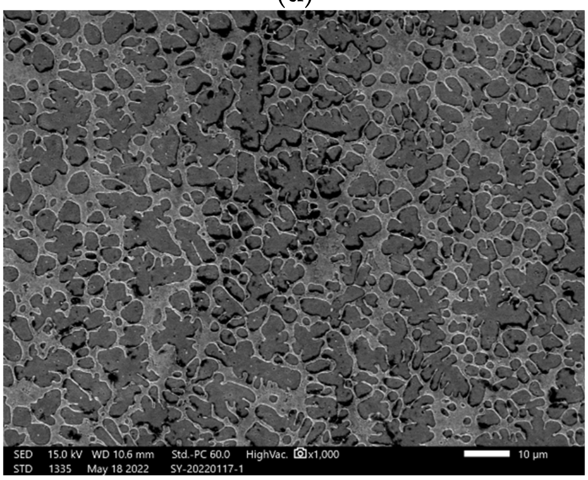

(**f**)

Figure 2. *Cont.*

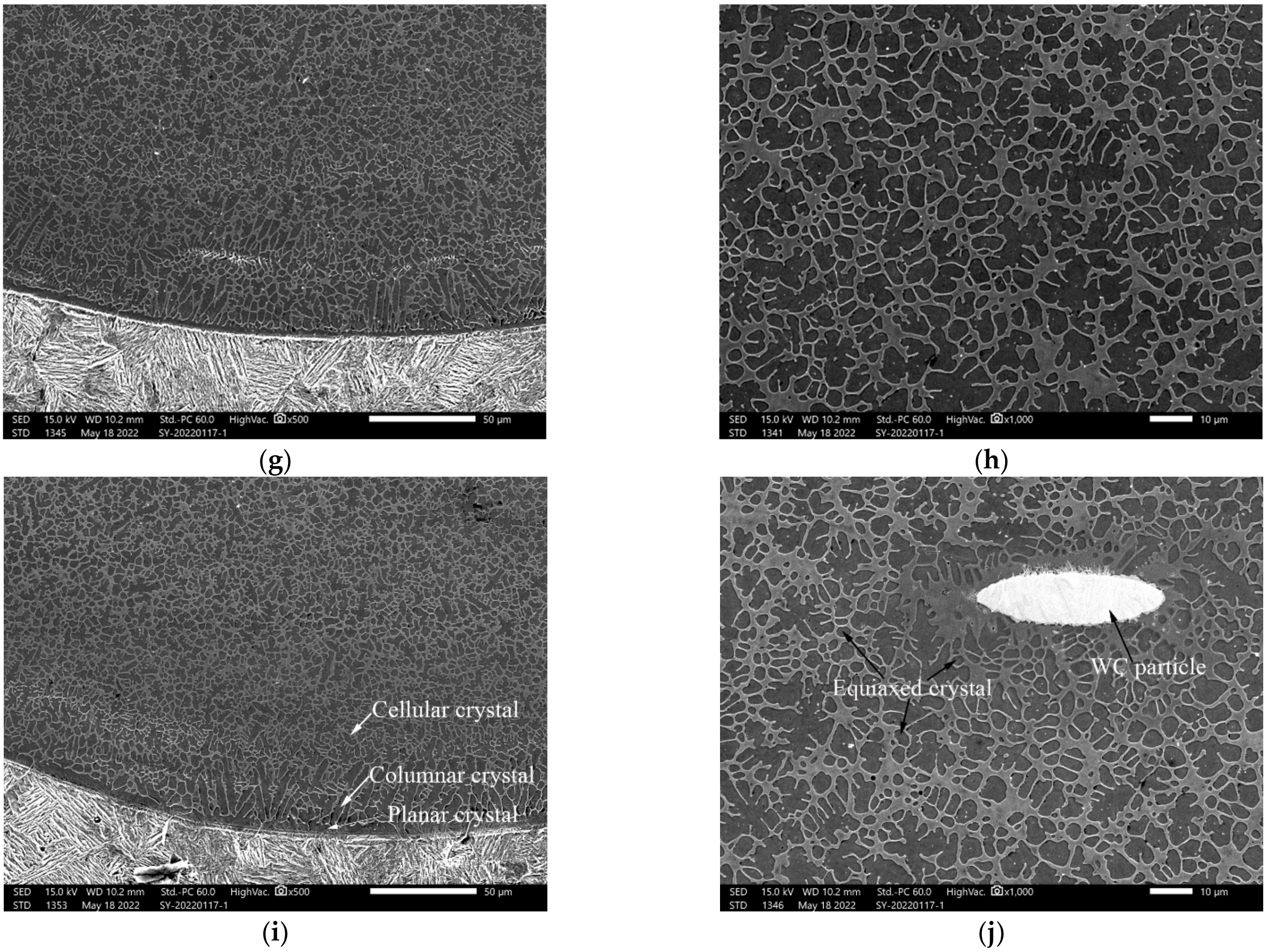

Figure 2. Microstructures of the composite coatings with different WC contents: (**a**,**b**) 0 wt.% WC; (**c**,**d**) 4 wt.% WC; (**e**,**f**) 8 wt.% WC; (**g**,**h**) 12 wt.% WC and (**i**,**j**) 16 wt.% WC.

EDS mapping was conducted for the coating with 8 wt.% WC addition and the result is shown in Figure 3. It is evident that W and C elements were segregated in the white region, suggesting the white region was a WC particle. The beard-like morphology appeared around the WC particle, indicating that the WC particle was partially melted. The partially melted WC particles revealed that the WC particles were metallurgically bonded with the Fe-based laser cladding coating matrix. The melting of WC particles led to the diffusion of W and C elements into the dendrite region. As a result, the W atoms dissolved into the matrix, which played a solid solution strengthening effect on the matrix. In addition, C and Cr elements were mainly distributed in the dendrite region, indicating that the dendrite region is mainly composed of chromium carbide. Figure 4 shows the elemental content of the area in Figure 3. The W content in this area was more than 8 wt.%, which is mainly due to the enrichment of WC particles in this area, so the W content here surpassed the nominal content (8 wt.%).

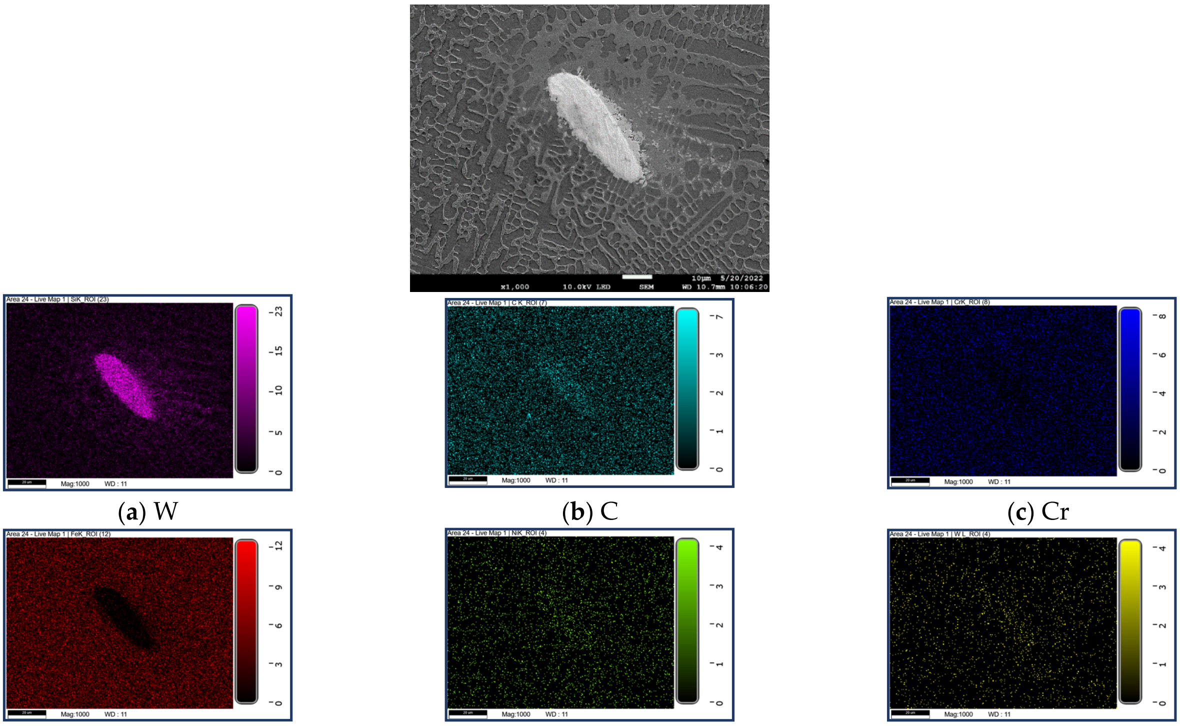

Figure 3. EDS mapping of the composite coating with 8 wt.% WC. (**a**) W element; (**b**) C element; (**c**) Cr element; (**d**) Fe element; (**e**) Ni element; (**f**) Si element

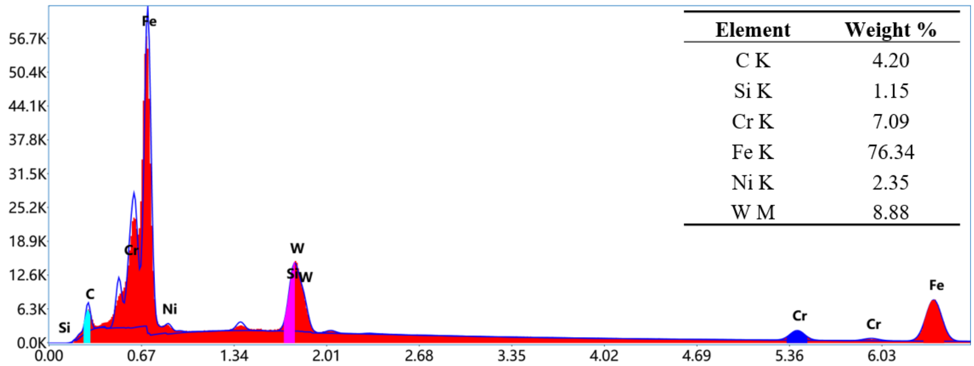

Figure 4. Chemical composition of the composite coating with 8 wt.% WC.

3.3. Microhardness

In order to investigate the effect of WC content on the microhardness of the coatings, the microhardness measurement was conducted, as shown in Figure 5. The microhardness of the coating without WC was recorded to be about 763.1 HV. With the increase of WC content, the microhardness of the cladding layer increases gradually. When the content of WC is 16 wt.%, the microhardness is about 826.2 HV, indicating that the addition of WC increased the microhardness of the coatings. This is mainly attributed to the following reasons: (1) The proportion of hard phase (i.e., WC and chromium carbide) in the coatings increased with the increase of WC content, which improved the microhardness of the coatings. (2) Part of the W atoms dissolved into the matrix, which played a solid solution strengthening role on the matrix and consequently increased the microhardness of the coating. (3) With WC addition, grain refinement was observed in the coatings. The refined grains improved the grain boundary density and inhibited the motion of dislocations. The microhardness of the Fe-based cladding coating increases gradually under these strengthening effects.

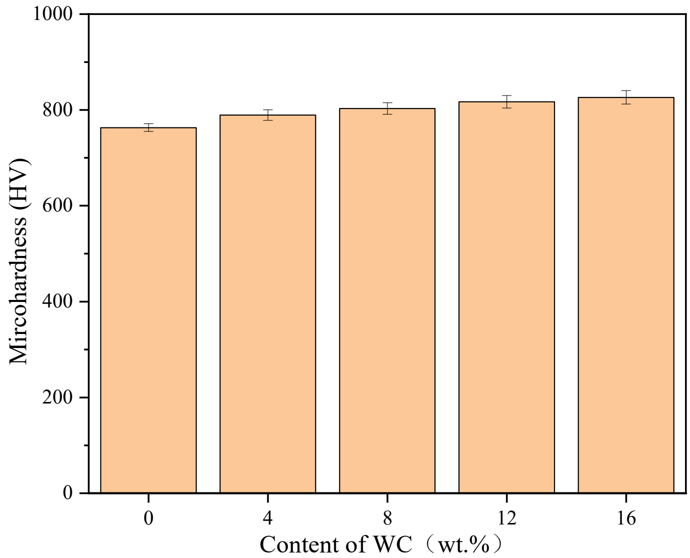

Figure 5. Microhardness of the composite coatings with different WC contents.

3.4. Wear Performance

Figure 6 shows the wear loss of the substrate and coatings with different WC content after the wear tests. With the increase of WC content in the coating, the wear weight loss of the coatings decreased gradually, which was due to the fact that the addition of WC improved the wear resistance of Fe-based coatings. It can be seen that the wear weight loss of the Q550 substrate was the largest and the wear weight losses of the coatings with different WC contents were less than that of the substrate. The relative wear resistance of the coating with 16 wt.% WC is approximately 16.3 and 9.7 times higher than those of the substrate and coating without WC, respectively. The enhanced wear resistance of the composite coatings benefited from their improved microhardness with WC addition, similar to results of previous researches [35–37].

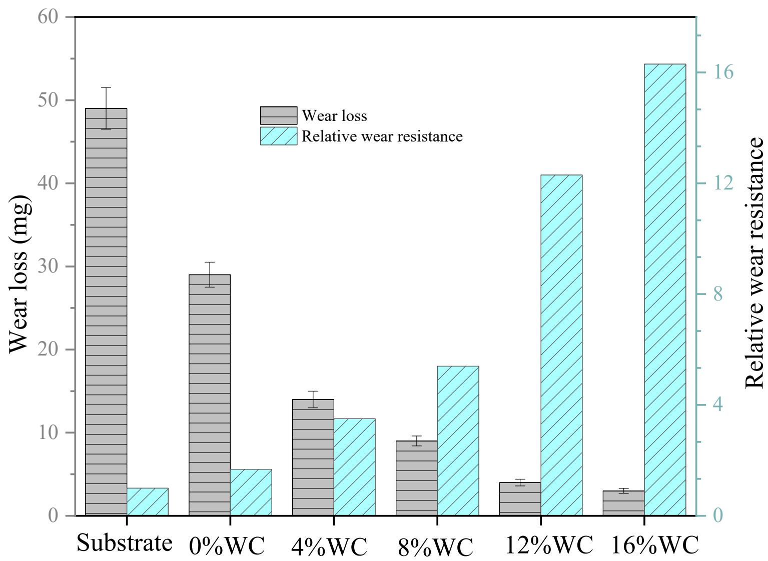

Figure 6. Wear loss and relative wear resistance of the composite coatings with different WC contents after wear tests.

Figure 7 shows the worn surface morphologies of the coatings with different WC contents. It can be seen that the wear track of the substrate was obviously wider than those of the composite coatings. In addition, with the increase of WC content, both the depth and width of the furrows inside the wear tracks decreased, suggesting an increased wear resistance of the coatings. The existence of furrows revealed that the wear mechanism of the coatings was mainly abrasive wear. As shown in Figure 7f, a white adhesion (position 1) appeared on the worn surface. According to the EDS results in Figure 8, the oxygen content in region 1 is relatively high. Therefore, it is identified as oxides. This is mainly due to the fierce contact between the grinding ball and the coating during the wear test process increasing the temperature of the contact surface, leading to the worn surface happened oxidation to some extent. The oxides formed on the worn surface could act as a lubricant and withstand wear [38], which further decreased the wear rate of the composite coatings.

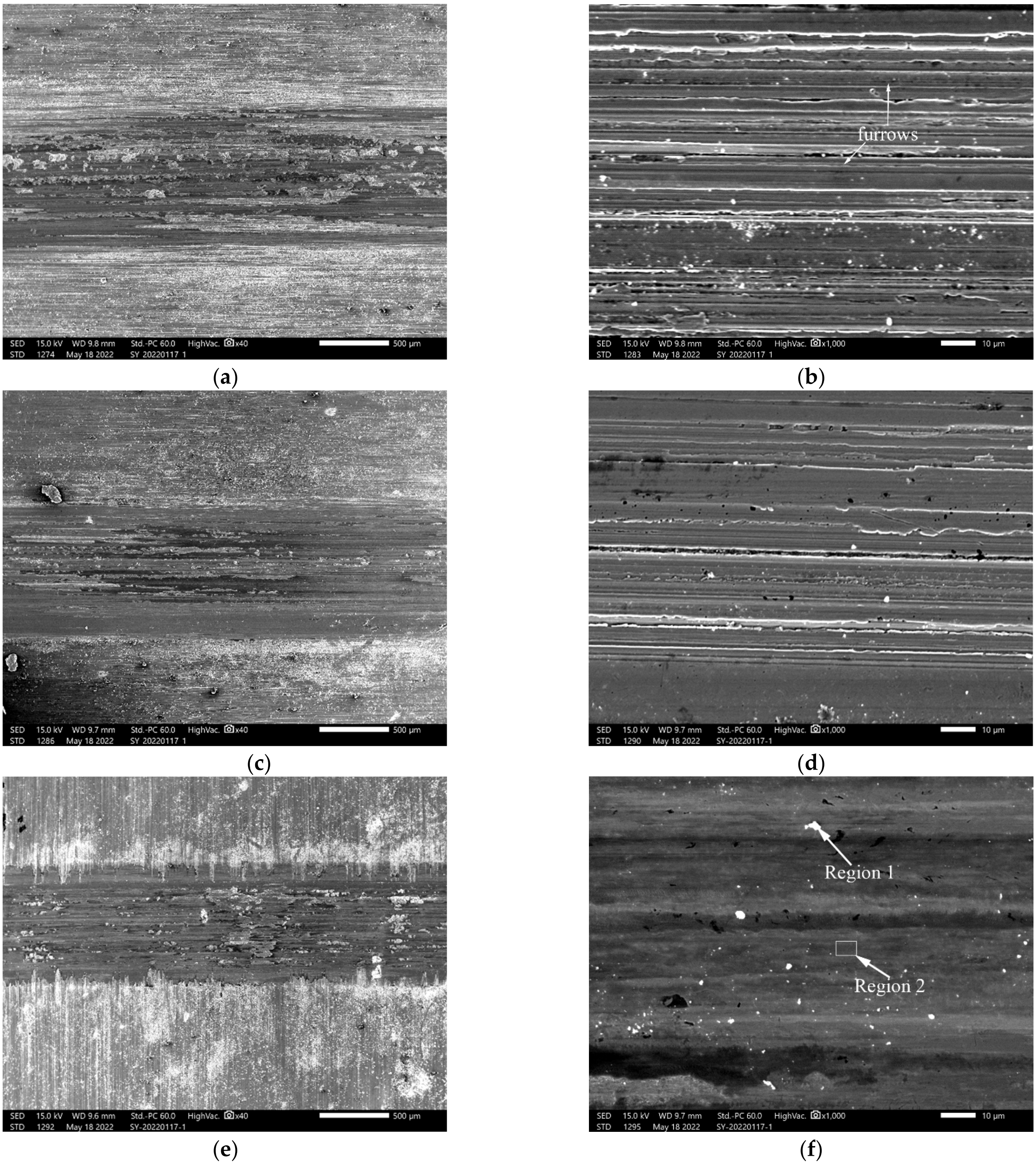

Figure 7. *Cont.*

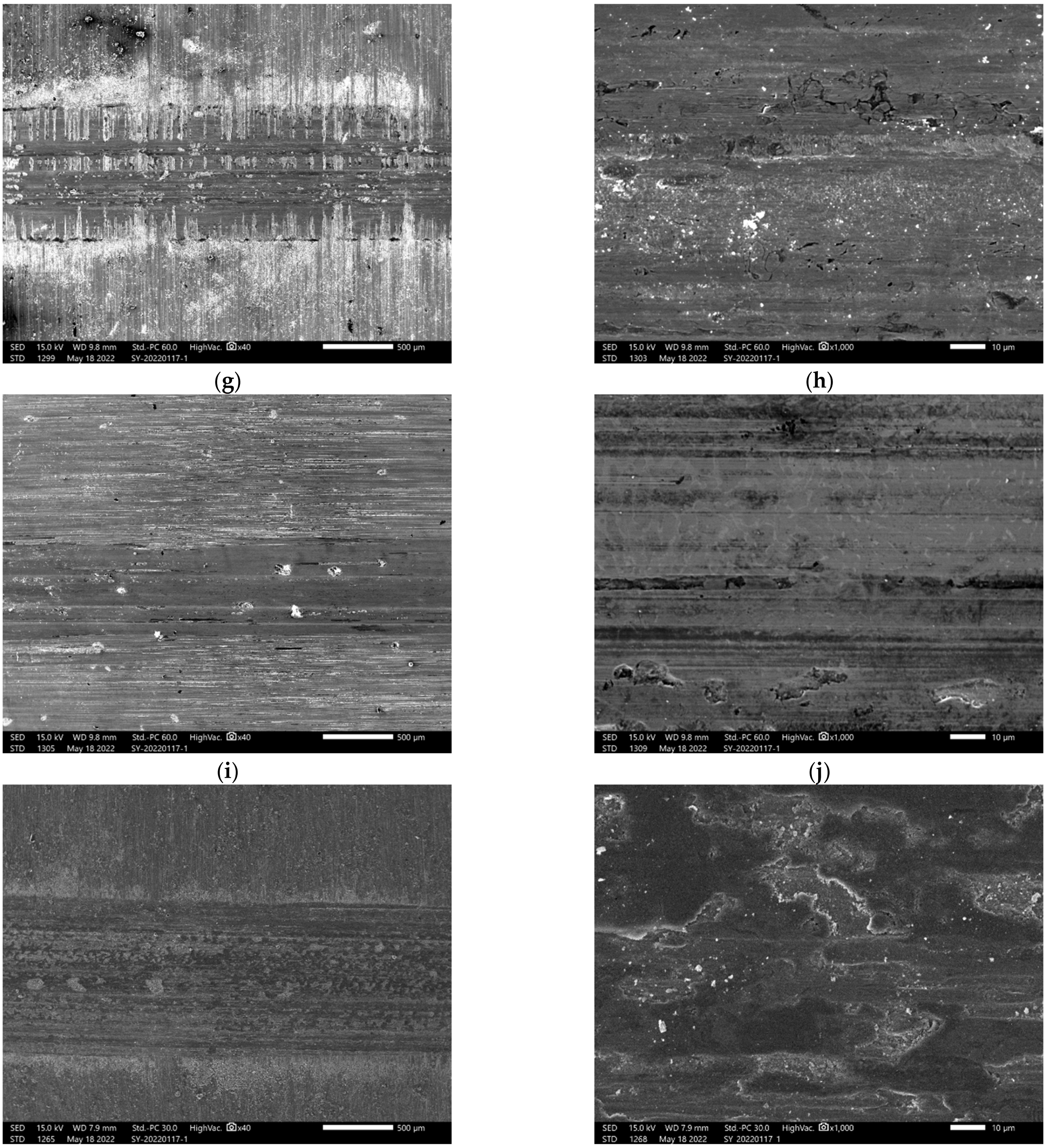

(**g**) (**h**)

(**i**) (**j**)

(**k**) (**l**)

Figure 7. Worn surface images of substrate and composite coatings with different WC contents: (**a**,**b**) 0 wt.% WC; (**c**,**d**) 4 wt.% WC; (**e**,**f**) 8 wt.% WC; (**g**,**h**) 12 wt.% WC; (**i**,**j**) 16 wt.% WC and (**k**,**l**) Q550 substrate.

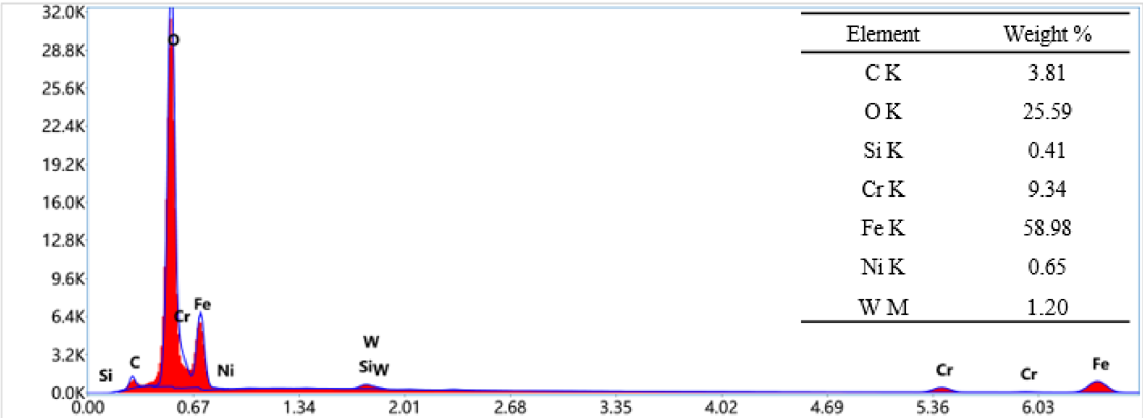

(**a**)

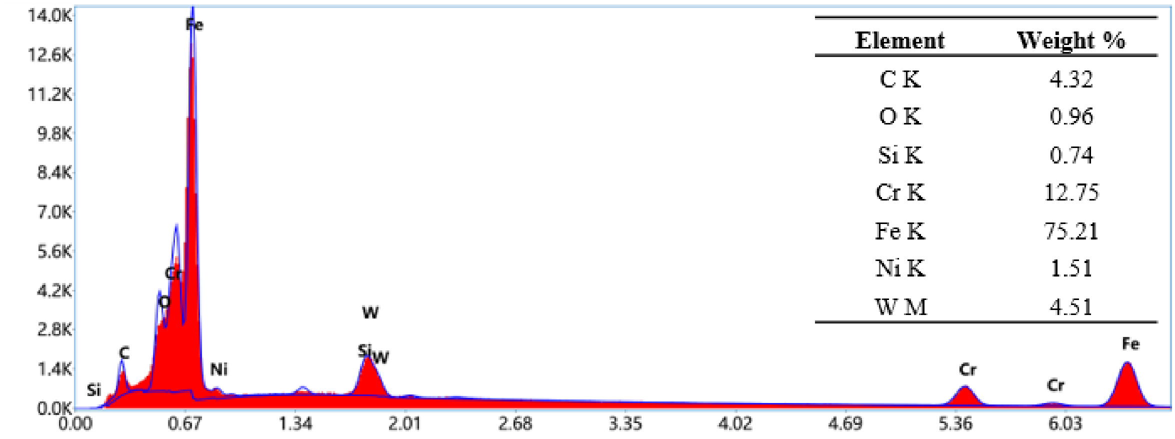

(**b**)

Figure 8. EDS results of regions in Figure 7f: (**a**) region 1 and (**b**) region 2.

Figure 9 shows the worn area of the grinding ball after the wear test. It can be seen that a small platform appears on the grinding ball (Figure 9a), suggesting that the grinding ball also underwent certain wear during the wear test. Furrows also appeared on the worn area of the grinding ball, which indicates the grinding ball underwent abrasive wear during the wear test. EDS analysis shows that the elements of region 2 contained a high oxygen content (Figure 9b,d) and the W element was detected on the worn area of the grinding ball (Figure 9d), which indicates that abrasive wear, oxidative wear and adhesion wear occurred on the grinding balls during the wear test.

The wear debris morphology is shown in Figure 10. The wear debris mainly consisted of long lumps and fine powders. The worn surface material was exfoliated or extruded from the surface to form three-body abrasive wear together with the coating and the grinding ball. Therefore, the wear debris was mainly powder-like [39]. In the EDS result, the oxygen content in the wear debris is high, indicating that the wear debris might be the peeled oxide layers [40], which further proves that oxidative wear occurred during the wear tests. A combination of Figures 7, 9 and 10 revealed that the wear mechanism of the coatings was mainly abrasive wear, along with slight adhesion wear and oxidative wear.

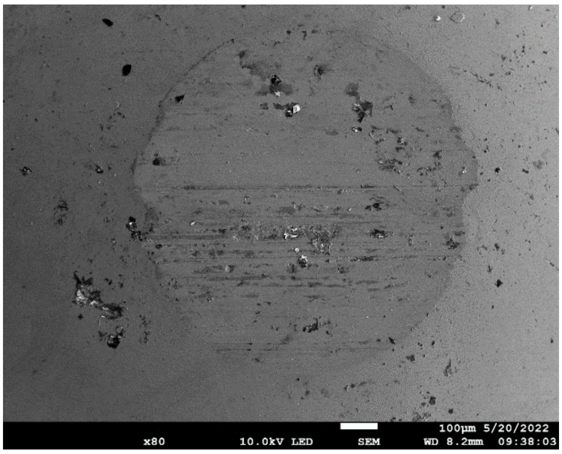

(**a**)

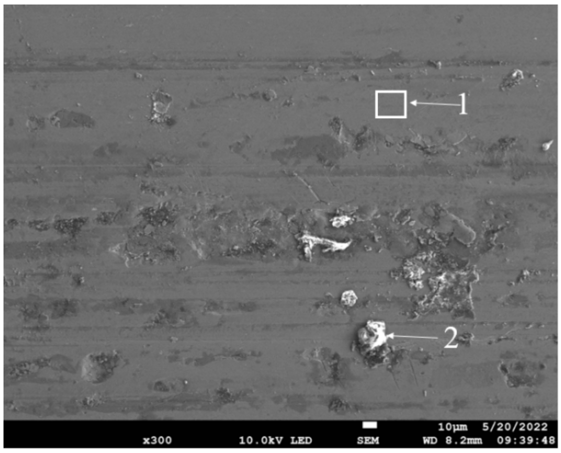

(**b**)

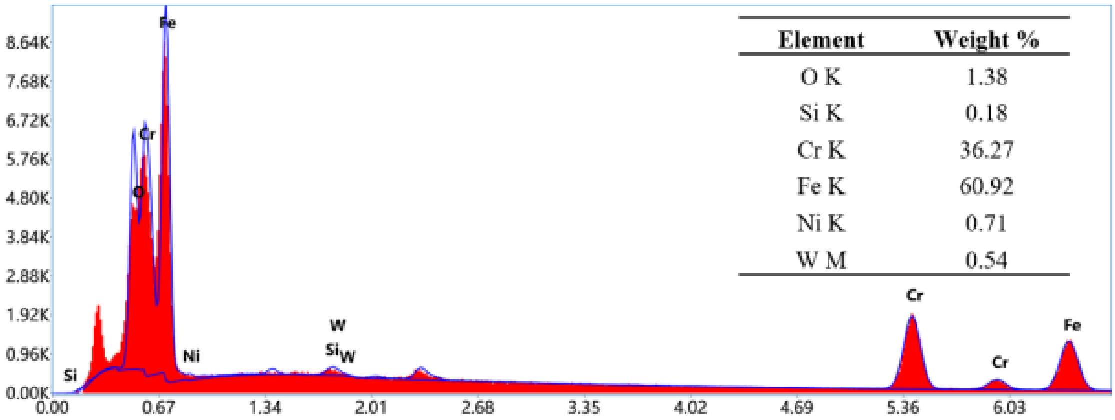

(**c**)

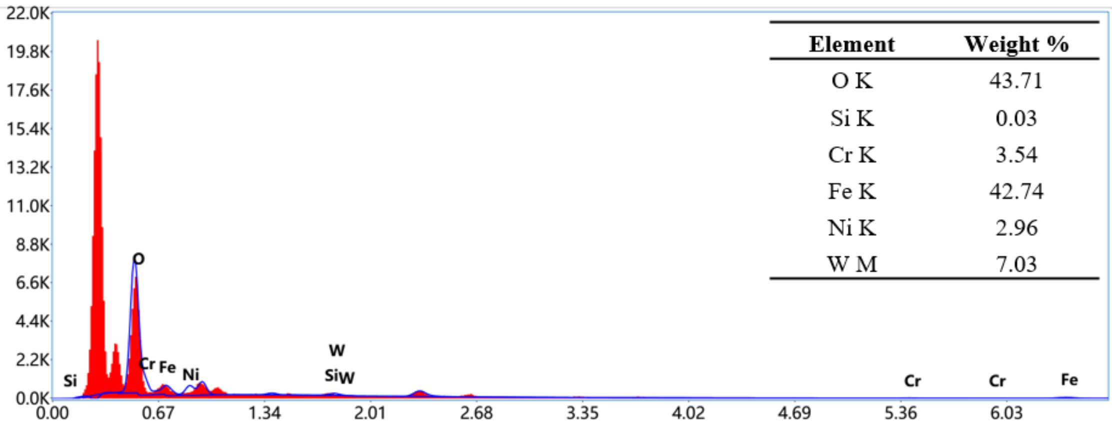

(**d**)

Figure 9. Worn surface of the grinding ball and corresponding EDS results: (**a**) low and (**b**) high magnified views of worn surface of the grinding ball; corresponding EDS results of (**c**) region 1 and (**d**) region 2 in (**b**).

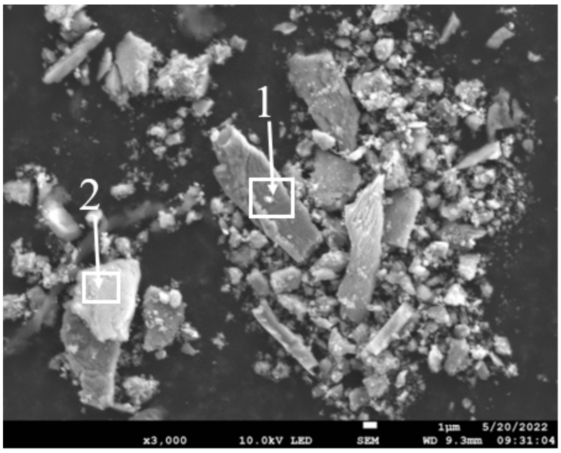

(**a**)

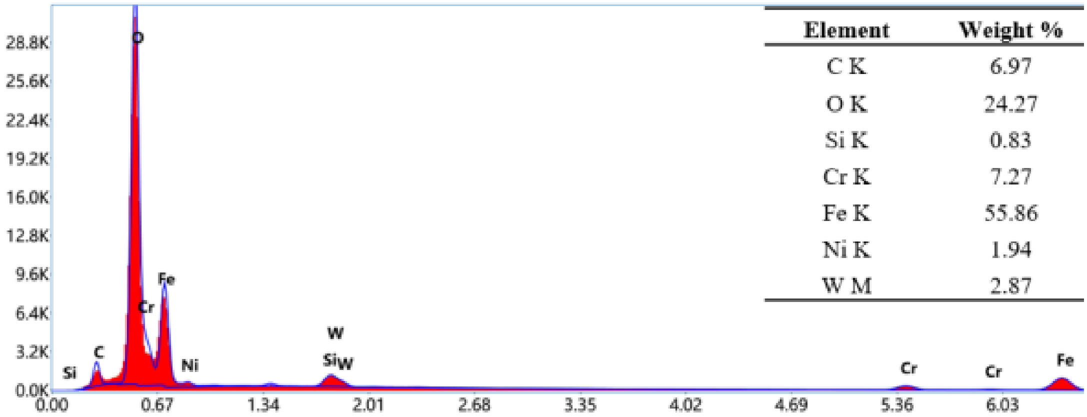

Element	Weight %
C K	6.97
O K	24.27
Si K	0.83
Cr K	7.27
Fe K	55.86
Ni K	1.94
W M	2.87

(**b**)

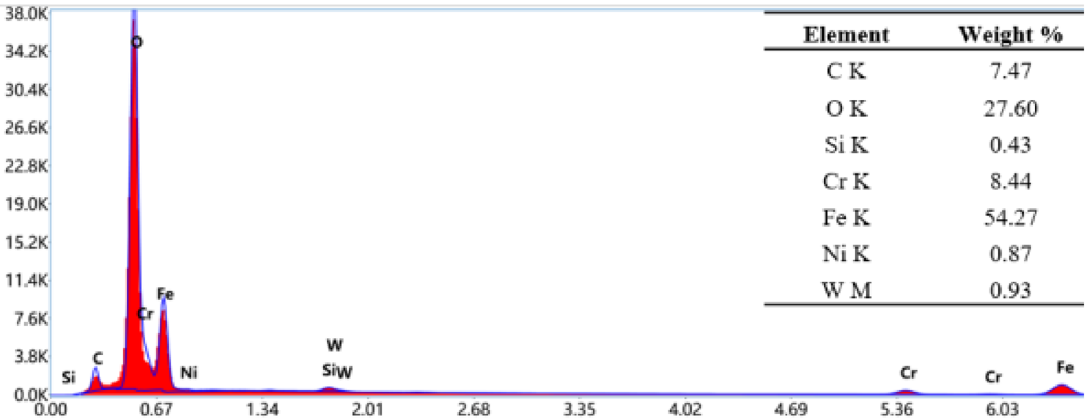

Element	Weight %
C K	7.47
O K	27.60
Si K	0.43
Cr K	8.44
Fe K	54.27
Ni K	0.87
W M	0.93

(**c**)

Figure 10. Wear debris and corresponding EDS results: (**a**) debris morphology; corresponding EDS results of (**b**) region 1 and (**c**) region 2 in (**a**).

4. Conclusions

In this study, the Fe-based coatings with different WC addition were fabricated via laser cladding to improve the wear resistance of the wind turbine gears. The morphology, composition, microhardness and wear resistance of the composite coating formed under different WC contents were studied, respectively. The main findings are summarized as follows:

(1) The microstructures of the regions above the fusion zone gradually changed from planar crystal to columnar crystal, cellular crystal and equiaxed crystals due to the ratio of temperature gradient (G) and solidification rate (R) changed in different zones. Moreover, the microstructure inside the coatings changed significantly with different amounts of WC addition. The grain size of the coatings gradually refined with increasing WC content.
(2) The addition of WC improved the microhardness of the coatings due to the proportion of hard phase, solid solution strengthening and grain refinement which increased with the increased of WC content.
(3) The wear weight loss decreased and the wear resistance increased with the increase of WC content in the Fe-based coatings. The enhanced wear resistance benefited from their improved microhardness with WC addition. The wear mechanism of the coatings was mainly abrasive wear, along with slight adhesion wear and oxidative wear.

Author Contributions: Conceptualization, formal analysis and writing—original draft, A.W.; Methodology, data curation and funding acquisition, Y.T., F.W. and S.Y.; Validation; Project administration and supervision, T.T.; Date analysis, writing—review and editing, supervision, K.W. All authors have read and agreed to the published version of the manuscript.

Funding: This research was funded by the Project Supported by China Huaneng Group (HNKJ21-HF257), the Changsha Municipal Natural Science Foundation (No. kq2202196) and the Tribology Science Fund of State Key Laboratory of Tribology (No. SKLTKF21B08).

Institutional Review Board Statement: Not applicable.

Informed Consent Statement: Not applicable.

Data Availability Statement: Not applicable.

Conflicts of Interest: The authors declare no conflict of interest.

References

1. Bejger, A.; Frank, E.; Bartoszko, P. Failure Analysis of Wind Turbine Planetary Gear. *Energies* **2021**, *14*, 6768. [CrossRef]
2. Tazi, N.; Châtelet, E.; Bouzidi, Y. Wear Analysis of Wind Turbine Bearings. *Int. J. Renew. Energy Res.* **2017**, *7*, 2120–2129.
3. Zhang, Y.; Zuo, T.T.; Tang, Z.; Gao, M.C.; Dahmen, K.A.; Liaw, P.K.; Lu, Z.P. Microstructures and properties of high-entropy alloys. *Prog. Mater. Sci.* **2014**, *61*, 1–93. [CrossRef]
4. Yang, Z.; Zheng, J.; Zhan, K.; Jiang, C.; Ji, V. Surface characteristic and wear resistance of S960 high-strength steel after shot peening combing with ultrasonic sprayed graphene oxide coating. *J. Mater. Sci. Technol.* **2022**, *18*, 978–989. [CrossRef]
5. Luchtenberg, P.; Campos, P.T.; Soares, P.; Laurindo, C.A.H.; Maranho, O.; Torres, R.D. Effect of welding energy on the corrosion and tribological properties of duplex stainless steel weld overlay deposited by GMAW/CMT process. *Surf. Coat. Technol.* **2019**, *375*, 688–893. [CrossRef]
6. Dorner-Reisel, A.; Reisel, G.; Seeger, J.; Svoboda, S.; Akhtar, W.A.A. Thermally sprayed coatings for protection of integrated sensor systems on tribological loaded surfaces. *Surf. Coat. Technol.* **2021**, *424*, 127619. [CrossRef]
7. Shengbin, Z.; Chenpeng, J.; Yuxue, Y.; Lixin, W.; Yiming, H.; Lijun, Y. Effects of laser remelting on microstructural characteristics of Ni-WC composite coatings produced by laser hot wire cladding. *J. Alloy. Compd.* **2022**, *908*, 164612. [CrossRef]
8. Zhao, S.; Xu, S.; Yang, L.; Huang, Y. WC-Fe metal-matrix composite coatings fabricated by laser wire cladding. *J. Mater. Process. Technol.* **2022**, *301*, 117438. [CrossRef]
9. Pelletier, J.M.; Sahour, M.C.; Pilloz, M.; Vannes, A.B. Influence of processing conditions on geometrical features of laser claddings obtained by powder injection. *J. Mater. Sci.* **1993**, *28*, 5184–5188. [CrossRef]
10. Meyer, F.; Mathieu, J.F.; Cesario, D.; Pelletier, J.M. Production of Ti/TiC dispersoid coatings on titanium base alloys by laser treatment. *Lasers Eng.* **1995**, *4*, 263.
11. Hidouci, A.; Pelletier, J.M. Microstructure and mechanical properties of MoSi2 coatings produced by laser processing. *Mater. Sci. Eng. A* **1998**, *252*, 17–26. [CrossRef]
12. Li, Y.; Wang, K.; Fu, H.; Guo, X.; Lin, J. Microstructure and wear resistance of in-situ TiC reinforced AlCoCrFeNi-based coatings by laser cladding. *Appl. Surf. Sci.* **2022**, *585*, 152703. [CrossRef]
13. Hidouci, A.; Pelletier, J.M.; Ducoin, F.; Dezert, D.; El Guerjouma, R. Microstructural and mechanical characteristics of laser coatings. *Surf. Coat. Technol.* **2000**, *123*, 17–23. [CrossRef]

14. Pelletier, J.M.; Sauger, E.; Gachon, Y.; Vannes, A.B. Mechanical and tribological properties of Hadfield steel coatings manufactured by laser processing. *J. Mater. Sci.* **1999**, *34*, 2955–2969. [CrossRef]
15. Li, Y.; Shi, Y. Microhardness, wear resistance, and corrosion resistance of $Al_xCrFeCoNiCu$ high-entropy alloy coatings on aluminum by laser cladding. *Opt. Laser. Technol.* **2021**, *134*, 106632. [CrossRef]
16. Cui, Y.; Shen, J.; Manladan, S.M.; Geng, K.; Hu, S. Wear resistance of $FeCoCrNiMnAl_x$ high-entropy alloy coatings at high temperature. *Appl. Surf. Sci.* **2020**, *512*, 145736. [CrossRef]
17. Jin, G.; Cai, Z.; Guan, Y.; Cui, X.; Liu, Z.; Li, Y.; Dong, M.; Zhang, D. High temperature wear performance of laser-cladded FeNiCoAlCu high-entropy alloy coating. *Appl. Surf. Sci.* **2018**, *445*, 113–122. [CrossRef]
18. Arif, Z.U.; Khalid, M.Y.; Al Rashid, A.; ur Rehman, E.; Atif, M. Laser deposition of high-entropy alloys: A comprehensive review. *Opt. Laser Technol.* **2022**, *145*, 107447. [CrossRef]
19. Zhu, L.; Xue, P.; Lan, Q.; Meng, G.; Ren, Y.; Yang, Z.; Xu, P.; Liu, Z. Recent research and development status of laser cladding: A review. *Opt. Laser. Technol.* **2021**, *138*, 106915. [CrossRef]
20. Wang, K.; Du, D.; Liu, G.; Pu, Z.; Chang, B.; Ju, J. A study on the additive manufacturing of a high chromium Nickel-based superalloy by extreme high-speed laser metal deposition. *Opt. Laser. Technol.* **2021**, *133*, 106504. [CrossRef]
21. Huebner, J.; Kata, D.; Kusiński, J.; Rutkowski, P.; Lis, J. Microstructure of laser cladded carbide reinforced Inconel 625 alloy for turbine blade application. *Ceram. Int.* **2017**, *43*, 8677–8684. [CrossRef]
22. Zhu, Y.; Yang, Y.; Mu, X.; Wang, W.; Yao, Z.; Yang. H. Study on wear and RCF performance of repaired damage railway wheels: Assessing laser cladding to repair local defects on wheels. *Wear* **2019**, *430–431*, 126–136. [CrossRef]
23. Wang, Q.; Qian, R.; Yang, J.; Niu, W.; Zhou, L.; Pan, X.; Su, C. Effect of high-speed powder feeding on microstructure and tribological properties of Fe-based coatings by laser cladding. *Coatings* **2021**, *11*, 1456. [CrossRef]
24. Lyu, Y.; Leonardi, M.; Mancini, A.; Wahlström, J.; Olofsson, U. Tribology and airborne particle emission of laser-cladded Fe-based coatings versus non-asbestos organic and low-metallic brake materials. *Metals* **2021**, *11*, 1703. [CrossRef]
25. Ju, J.; Shen, Z.; Kang, M.; Zhang, J.; Wang, J. On the preferential grain boundary oxidation of a Ni-Co-based superalloy. *Corros. Sci.* **2022**, *199*, 110203. [CrossRef]
26. Wang, K.; Du, D.; Liu, G.; Pu, Z.; Chang, B.; Ju, J. Microstructure and mechanical properties of high chromium nickel-based superalloy fabricated by laser metal deposition. *Mat. Sci. Eng. A* **2020**, *780*, 139185. [CrossRef]
27. Liu, R.; Zhang, M.; Yu, J.; Yang, Q.; Gao, S. Microstructural transformation and high-temperature aluminum corrosion properties of Co-based alloy coating prepared by laser cladding. *Coatings* **2022**, *12*, 603. [CrossRef]
28. Liu, X.; Bi, J.; Meng, Z.; Ke, Y.; Li, R.; Zhang, T. Development of Co-based amorphous composite coatings synthesized by laser cladding for neutron shielding. *Materials* **2021**, *14*, 279. [CrossRef]
29. Chen, H.; Lu, Y.; Sun, Y.; Wei, Y.; Wang, X.; Liu, D. Coarse TiC particles reinforced H13 steel matrix composites produced by laser cladding. *Surf. Coat. Technol.* **2020**, *395*, 125867. [CrossRef]
30. Ding, H.; Mu, X.; Zhu, Y.; Yang, W.; Xiao, Q.; Wang, W.; Liu, Q.; Guo, J.; Zhou, Z. Effect of laser claddings of Fe-based alloy powder with different concentrations of WS_2 on the mechanical and tribological properties of railway wheel. *Wear* **2022**, *488–489*, 204174. [CrossRef]
31. Chen, L.; Yu, T.; Guan, C.; Zhao, Y. Microstructure and properties of metal parts remanufactured by laser cladding TiC and TiB_2 reinforced Fe-based coatings. *Ceram. Int.* **2022**, *48*, 14127–14140. [CrossRef]
32. Huang, Y.; Hu, Y.; Zhang, M.; Mao, C.; Wang, K.; Tong, Y.; Zhang, J.; Li, K. Multi-objective optimization of process parameters in laser cladding CoCrCuFeNi high-entropy alloy coating. *J. Therm. Spray Technol.* **2022**, 1–16. [CrossRef]
33. Wang, C.; Zhang, S.; Zhang, C.H.; Wu, C.L.; Zhang, J.B.; Abdullah, A.O. Phase evolution and wear resistance of in situ synthesized V_8C_7 particles reinforced Fe-based coating by laser cladding. *Opt. Laser Technol.* **2018**, *105*, 58–65. [CrossRef]
34. Wu, Z.; Li, T.; Li, Q.; Shi, B.; Li, X.; Wang, X.; Lu, H.; Zhang, H. Process optimization of laser cladding Ni60A alloy coating in remanufacturing. *Opt. Laser Technol.* **2019**, *120*, 105718. [CrossRef]
35. Ma, G.; Cui, H.; Jiang, D.; Chen, H.; Hu, X.; Zhang, G.; Wang, R.; Sun, X.; Song, X. The evolution of multi and hierarchical carbides and their collaborative wear-resisting effects in CoCrNi/WC composite coatings via laser cladding. *Mater. Today Commun.* **2022**, *30*, 103223. [CrossRef]
36. Li, W.; Yang, X.; Xiao, J.; Hou, Q. Effect of WC mass fraction on the microstructure and friction properties of WC/Ni60 laser cladding layer of brake discs. *Ceram. Int.* **2021**, *47*, 28754–28763. [CrossRef]
37. Wang, T.; Zhu, L.; Song, H.; Wang, H. Effect of WC-17Co content on microstructure and properties of IN718 composites prepared by laser cladding. *Opt. Laser. Technol.* **2022**, *148*, 107780. [CrossRef]
38. Du, L.M.; Lan, L.W.; Zhu, S.; Yang, H.J.; Shi, X.H.; Liaw, P.K.; Qiao, J.W. Effects of temperature on the tribological behavior of $Al_{0.25}CoCrFeNi$ high-entropy alloy. *J. Mater. Sci. Technol.* **2019**, *35*, 917–925. [CrossRef]
39. Zhu, Y.; Liu, X.-B.; Liu, Y.-F.; Wang, G.; Wang, Y.; Meng, Y.; Liang, J. Development and characterization of Co-Cu/Ti_3SiC_2 self-lubricating wear resistant composite coatings on Ti_6Al_4V alloy by laser cladding. *Surf. Coat. Technol.* **2021**, *424*, 127664. [CrossRef]
40. Liu, Y.-F.; Zhuang, S.-G.; Liu, X.-B.; OuYang, C.-S.; Zhu, Y.; Meng, Y. Microstructure evolution and high-temperature tribological behavior of Ti_3SiC_2 reinforced Ni60 composite coatings on 304 stainless steel by laser cladding. *Surf. Coat. Technol.* **2021**, *420*, 127335. [CrossRef]